3D Slab Selective AFI utilizing a thin slab approach

C. T. Sica[1], and C. M. Collins[1]
[1]Radiology, The Pennsylvania State University, Hershey, Pennsylvania, United States

Introduction: AFI [1] is a well established B_1^+ mapping technique. One drawback of AFI is the influence of slice profile effects on the flip angle calculation, which necessitates the usage of spatially non-selective RF pulses and concomitant full 3D encoding and imaging of the target volume, resulting in significant scan durations. A previous effort to remove the necessity of full-volume excitation examined the accuracy of AFI utilizing slice selective Gaussian and SLR pulses [2]. Another approach discussed in Ref [1] is to utilize a slab-selective pulse and restrict imaging to the flat portion of the slab profile. Here we utilize a sinc pulse to excite a slab that is thicker than the target slice but much thinner than the whole volume, followed by 3D encoding and imaging of the slab. The slices acquired on the relatively flat, central area of the excited slab are assumed accurate and slices on the outer edge of the slab are discarded, due to their corruption by slice profile effects. Encoding a small number of slices (4-8) across the slab significantly reduces the scan duration compared to a non-selective acquisition. This work compares the accuracy of 3D slab selective AFI with 3D non-selective AFI through simulation and experiments in a phantom.

Methods: Simulation: The RF and gradient waveforms for the slab-selective sinc pulse and non-selective hard pulse were exported from the Siemens pulse programming environment to IDL. Both RF pulses were calibrated to achieve a nominal 60 degree flip angle. The amplitude of the sinc pulse was then scaled from 7.6% to 143% of the nominal value in 29 steps, followed by numerical integration of the Bloch equations to obtain a series of 29 flip angle profiles. These flip angle profiles ranged from 5 degrees to 85 degrees. A 4 mm thick, central portion of each flip angle profile was extracted and substituted into the equations for S_1 and S_2 (Eqs. 1 to 6 from Ref. [1]) to obtain signal profiles $S_1(z)$ and $S_2(z)$. The signal profiles $S_1(z)$ and $S_2(z)$ were integrated and the quantity R was computed as $R = \int S_2(z)dz / S_1(z)dz$. The final simulated flip angles (29 total) were computed as Alpha = acos(5 * R - 1 / 5 - R), assuming a ratio of 5 for TR_2/TR_1. A similar series of steps were carried out for the hard RF pulse to compute a second series of simulated flip angles, and the results of the two simulations were plotted against one another.

Experimental: AFI scans were acquired on a Siemens 3T TIM Trio with a spherical Siemens water phantom (1.25g NiSO4 · 6H2O). T_1 of the phantom is approximately 290 ms. Reception utilized an eight channel head coil and transmission utilized the TIM Trio body coil. In-plane scan matrix and FOV were identical for the two techniques – 80 x 96 and 200 x 240 mm FOV. The full 3D scan acquired 52 partitions across a 208 mm FOV and utilized a 300 us hard RF pulse. The slab selective 3D scan acquired 8 partitions across a 32 mm FOV and utilized a 2 ms sinc pulse (see Figure 1). Both AFI scans utilized a nominal 60 degree flip angle, 25 ms TR_1, TR_2/TR_1 ratio of 5. Spoiling was implemented as described in Nehrke [3], using values of 129.3 degrees for the RF spoiling increment and 375/1875 mT/m * ms for the gradient spoiler area during TR_1 and TR_2 respectively.

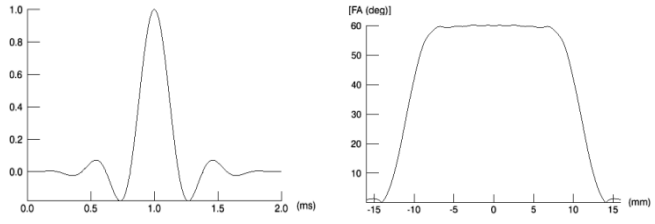

Figure 1: On the left, the slab selective sinc pulse utilized (normalized to 1). On the right, the profile for a nominal flip angle of 60 degrees.

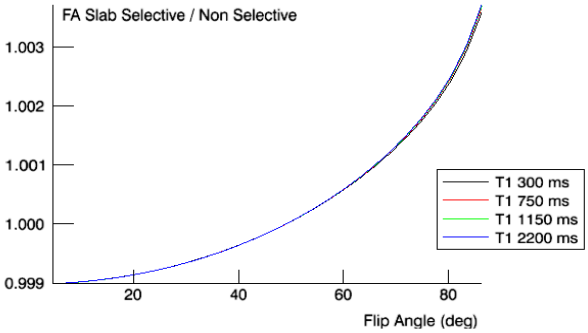

Figure 2: Simulation results. The ratio of the flip angle predicted by 3D non selective AFI to that predicted by 3D slab selective AFI is displayed for a range of flip angles and variety of T_1 values. Error remains within +0.5 to -0.5% across a wide range of cases.

Results: The slab selective sinc pulse and corresponding 60 degree flip angle profile are displayed in Fig.1. The simulation results are displayed in Figure 2. The simulation was repeated 4 times at several different T_1 values. For each of the 29 simulated flip angle profiles, the ratio of the flip angle predicted by 3D non selective AFI by the flip angle predicted by 3D slab selective AFI is computed. Figure 3 displays the experimental results. The 3D non selective AFI flip angle map is on the left, slab selective 3D AFI flip angle map in the middle, and the subtraction of the two on the right. Error remains within -0.5 to 0.5 degrees over the majority of the phantom. The acquisition time for the 3D non-selective was 10:24 for the AFI scan and 1:36 for the 3D slab selective AFI scan.

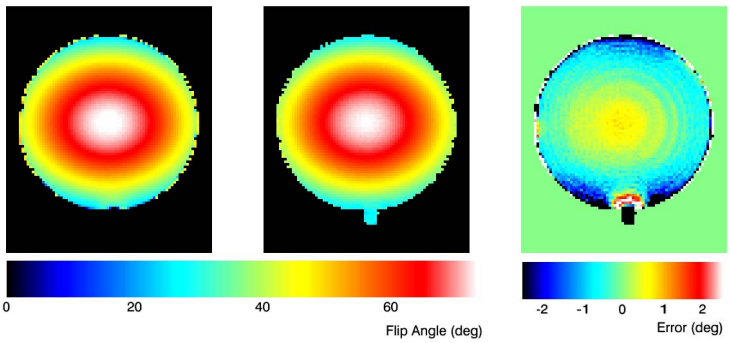

Figure 3: Experimental results. On the left, the flip angle map acquired with 3D non selective AFI. In the middle, the flip angle map acquired with 3D slab selective AFI. On the right, the subtraction of the left and middle flip angle maps.

Discussion: The agreement between the flip angles computed by 3D non-selective AFI and 3D slab selective AFI is excellent in both experiment and simulation. Despite the sinc pulse producing flip angle profiles with some degree of ripple, subsequent integration of these profiles and computation via AFI yielded very little error. A number of approaches are under investigation to further this work. The slab selective pulse utilized was a basic sinc pulse, and better performance may be possible with an SLR pulse. Varying the number of encoded slices across the slab and the thickness of the slab are also under consideration to decrease acquisition time and improve accuracy. Off-resonance across the slab profile during slab excitation will affect the accuracy of this method and requires a careful choice of the excitation pulse. Ref [1] investigates the performance of an SLR pulse in the context of off-resonance behavior and recommends a high bandwidth excitation pulse to reduce off-resonance sensitivity. In this work, the performance of a slab selective sinc was investigated in the context of B_1^+ inhomogeneity and its effect on the slab profile. An in-vivo implementation of this technique is also forthcoming.

References:

[1] Yarnykh V. Magn Reson Med 2007; 57:192-200 [2] Wu et al. P.ISMRM 2009, p.372 [3] Nehrke K. Magn Reson Med 2009; 61:84-92

Acknowledgements: We are grateful for support from NIH R01 EB000454.